# Single Ru(II) ions on ceria as a highly active catalyst for abatement of NO

| | |
|---|---|
| Journal: | *Journal of the American Chemical Society* |
| Manuscript ID | ja-2022-098733.R2 |
| Manuscript Type: | Article |
| Date Submitted by the Author: | 01-Feb-2023 |
| Complete List of Authors: | Khivantsev, Konstantin; Pacific Northwest National Laboratory,<br>Jaegers, Nicholas; Pacific Northwest National Laboratory<br>Aleksandrov, Hristiyan; University of Sofia, Faculty of Chemistry,<br>Song, Inhak; PNNL,<br>Pereira-Hernandez, Xavier; Pacific Northwest National Laboratory<br>Engelhard, Mark; Pacific Northwest National Laboratory, EMSL<br>Tian, Jinshu; Pacific Northwest National Laboratory<br>Chen, Linxiao; Pacific Northwest National Laboratory<br>Meira, Debora; Canadian Light Source Inc,<br>Kovarik, Libor; Environmental Molecular Sciences Laboratory<br>Vayssilov, Georgi; University of Sofia, Faculty of Chemistry and Pharmacy<br>Wang, Yong; Pacific Northwest National Laboratory,<br>Szanyi, János; Pacific Northwest National Laboratory, Institute for Integrated Catalysis |
| | |

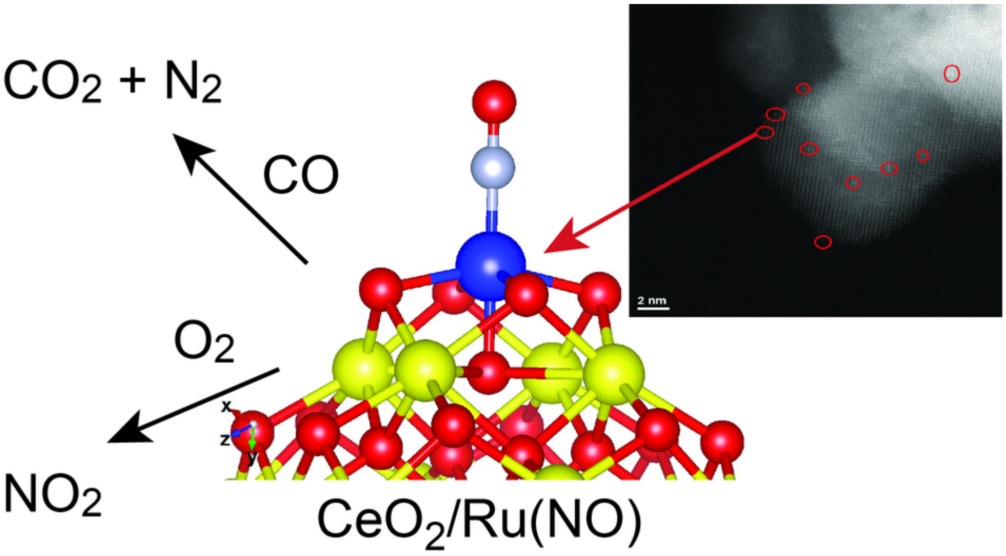

ruthenium ions dispersed on ceria are highly active for storage and catalytic abatement of environmental pollutant nitric oxide NO

80x45mm (300 x 300 DPI)

# Single Ru(II) ions on ceria as a highly active catalyst for abatement of NO

Konstantin Khivantsev,[a]* Nicholas R. Jaegers,[a] Hristiyan A. Aleksandrov,[b]* Inhak Song,[a] Xavier Isidro Pereira-Hernandez,[a] Mark H. Engelhard,[a] Jinshu Tian[a], Linxiao Chen[a], Debora Motta Meira[c], Libor Kovarik,[a] Georgi N. Vayssilov,[b] Yong Wang[a]* and János Szanyi[a]*

[a] Dr. Konstantin Khivantsev, Dr. Libor Kovarik, Dr. Nicholas R. Jaegers, Dr. Inhak Song, Dr. Jinshu Tian, Dr. Xavier I. Pereira Hernandez, Dr. Linxiao Chen, Dr. Yong Wang, Dr. Janos Szanyi,
Institute for Integrated Catalysis
Pacific Northwest National Laboratory
Richland, WA 99352 USA
Emails (correspondence to): Konstantin.Khivantsev@pnnl.gov, Haa@chem.uni-sofia.bg, Yong.Wang@pnnl.gov, Janos.Szanyi@pnnl.gov

[b] Professor Hristiyan A. Aleksandrov, Professor Georgi N. Vayssilov, Sofia University "St. Kliment Ohridski", Faculty of Chemistry and Pharmacy
1, J. Bourchier blvd, 1126, Sofia, Bulgaria

[c] Dr. Debora Motta Meira, CLS@APS, Advanced Photon Source, Argonne National Laboratory, 9700 S. Cass Avenue, Argonne, IL 60439, USA

**Abstract:** Atom trapping leads to catalysts with atomically dispersed $Ru_1O_5$ sites on (100) facets of ceria, as identified by spectroscopy and DFT calculations. This is a new class of ceria-based materials with Ru properties drastically different from the known M/ceria materials. They show excellent activity in catalytic NO oxidation, a critical step that requires use of large loadings of expensive noble metals in diesel aftertreatment systems. $Ru_1/CeO_2$ is stable during continuous cycling, ramping and cooling as well as presence of moisture. Furthermore, $Ru_1/CeO_2$ shows very high $NO_x$ storage properties due to formation of stable Ru-NO complexes as well as high spill-over rate of $NO_x$ onto $CeO_2$. Only ~0.05 wt% of Ru is required for excellent $NO_x$ storage. $Ru_1O_5$ sites exhibit much higher stability during calcination in air/steam up to 750 ºC in contrast to $RuO_2$ nanoparticles. We clarify the location of Ru(II) ions on the ceria surface and experimentally identify mechanism of NO storage and oxidation using DFT calculations and in-situ DRIFTS/Mass-spectroscopy. Moreover, we show excellent reactivity of $Ru_1/CeO_2$ for NO reduction by CO at low temperatures: only 0.1-0.5 wt% of Ru is sufficient to achieve high activity. Modulation-excitation in-situ infrared and XPS measurements reveal the individual elementary steps of NO reduction by CO on an atomically dispersed Ru ceria catalyst, highlighting unique properties of $Ru_1/CeO_2$ and its propensity to form oxygen vacancies/$Ce^{+3}$ sites that are critical for NO reduction, even at low Ru loadings. Our study highlights the applicability of novel ceria-based single-atom catalysts to NO and CO abatement.

**Introduction**. Air pollution is one of the main issues to tackle in environmental science and catalysis [1-3]. Deteriorating air quality is directly related to toxic $NO_x$ emissions, the majority of which are produced by vehicles exhaust. There clearly exists the urgent need to decrease emissions from engines and develop catalytic materials for NOx abatement based on less expensive (noble) metals with improved atom economy. NO oxidation is critical for environmental catalysis in diesel aftertreatment systems because $NO_2$ formation is important in lean $NO_x$ reduction [34-38]. Furthermore, $NO_2$ facilitates ammonia selective catalytic reduction (SCR) (so-called "fast" SCR, with an ideal 1:1 ratio between NO and $NO_2$) and lean $NO_x$ storage (in this case, NO must first be oxidized to $NO_2$ in order to be stored on LN traps materials). Best catalysts for NO oxidation typically contain a few wt% percent of expensive Pt and Pd [34-38]. Pt currently costs ~1,000 USD/ounce whereas Pd costs ~ 2,600 USD/ounce (note that Pt is approximately ~2 times heavier, so per molar basis the price is only ~1.3 higher for Pd than for Pt).

## Results and Discussion

**Anchoring Pt, Pd and Ru ions to ceria support.** In recent decade, the so-called single-atom materials with efficient utilization of single metal atoms/ions have been introduced that may offer promising alternatives and unusual reactivities compared to traditional nanoparticle catalysts. For example, thermally stable atomically dispersed Pt materials on ceria have been prepared via atom trapping approach at 800 ºC [28-31]. We now extended this synthesis to Pd. We also turned our attention to another transition metal ruthenium whose current price is ~500 USD per ounce and whose molecular weight is similar to that of Pd and Rh (Rh, on the other hand, costs ~15,000 USD per ounce, almost ~30 times more on the molar basis than Ru; Ru is approx ~4 times cheaper on per-molar basis than Pt and Pd; although it is important to note that the general noble metal prices are volatile and are subject to supply/demand issues, the price trends generally hold within the last decade; therefore, it is also beneficial not only to utilize a less expensive metal but also to diversify the catalytic portfolio. Taking advantage of the atom trapping approach, we prepared isolated Pd, Pt and Ru atoms on ceria in ~ equivalent molar amounts (atom loading per surface area of ceria) with 1 wt% Pt, 0.5 wt% Ru and 0.5 wt% Pd on ceria. We note that ceria materials with isolated Ru(II) have not been prepared or characterized before as well as shown to have advantageous catalytic properties. We observed pronounced stabilization of ceria surface area after heating at 800 ºC and producing atomically dispersed M/Ceria materials as opposed to undoped ceria (Tab. S1), in agreement with previous studies [42,72,73]. Anchoring these ions onto ceria produces stable materials that can survive heating in air at 800 ºC in agreement with our latest findings [42]. HAADF-STEM images of Pd, Pt and Ru supported ceria materials (Fig. 1, Figs S1-S5) show crystalline ceria nanoparticles with no noble metal nanoparticles. In the case of Pt on ceria we can identify single Pt atoms located on the

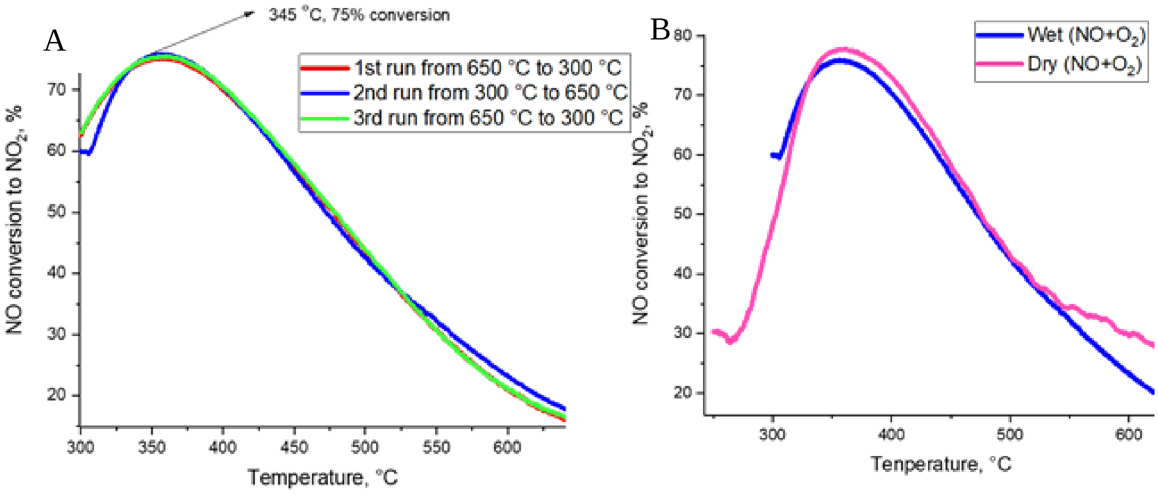

*Figure 1. NO oxidation performance of A. 0.5 wt% Ru/CeO$_2$(3 continuous runs from 650 to 300, showing stable NO oxidation performance in the presence of ~ 3% $H_2O$, 120 mg catalyst, 470 ppm NO, 13% $O_2$, total flow 300 sscm/min, GHSV ~ 150 L/g*hr. B. Comparison of wet and dry NO oxidation on aged 0.5 wt% Ru/CeO$_2$ up to 650 $^0$C (conditions are identical to A; dry experiments were carried out with the same NO and oxygen concentrations.*

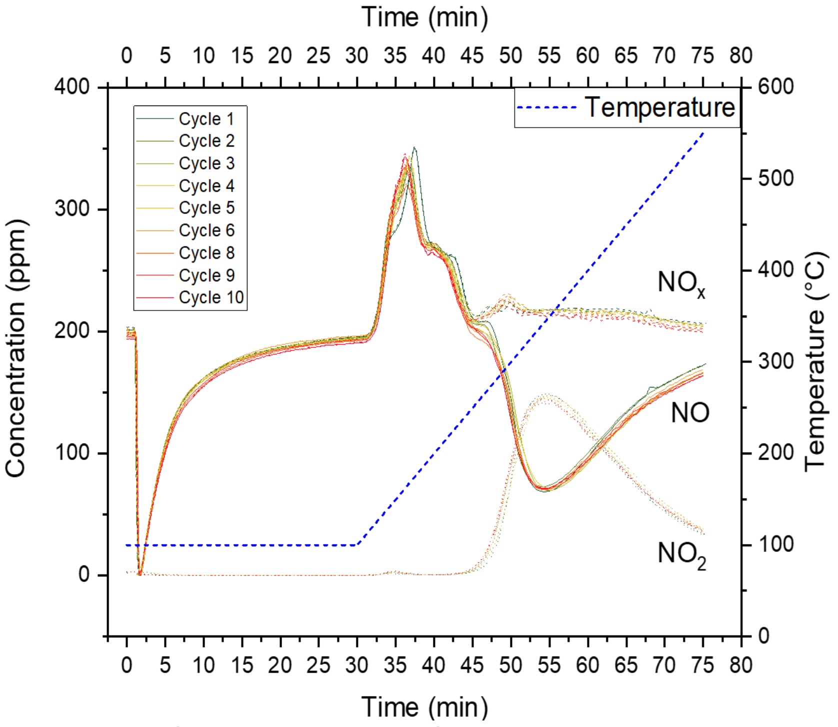

| Cycle | µmol NOx | mol NOx/mol Ru |
|---|---|---|
| 1 | 23.57 | 4.76 |
| 2 | 23.09 | 4.67 |
| 3 | 22.49 | 4.55 |
| 4 | 22.51 | 4.55 |
| 5 | 22.75 | 4.60 |
| 6 | 22.76 | 4.60 |
| 8 | 22.71 | 4.59 |
| 9 | 22.60 | 4.57 |
| 10 | 22.93 | 4.64 |

*Figure 2. Performance and stability of 0.25wt.% Ru$_1$/CeO$_2$ during sequential cycles of low-temperature NOx adsorption and NO oxidation. Gas composition was 200 ppm of NO, 2000 ppm CO, 12% $O_2$, ~3% $H_2O$, balanced with $N_2$. 120 mg catalyst was used with GHSV ~ 150 L/g*hr. Adsorption experiments were performed at 100 $^0$C. The temperature ramp (10 $^0$C/min) was started at a 30 minute mark; up to 550 $^0$C. NOx storage is shown per 120 mg catalyst. On average the stored NOx amount is ~ 190 micromoles/gram.*

surface of ceria (Fig. 1, Figs S1-S5). However, in the case of Pd and Ru, although the contrast is poor, on sufficiently thin parts of ceria nanoparticles tilted slightly off the zone-axis (to decrease scattering from bright Ce atom columns), we could in fact identify single Ru atoms (shown by arrows on the surface of different ceria crystallites in Fig. S5). In all 3 cases, EDS maps clearly reveal presence of Pd, Pt and Ru well-dispersed throughout the sample, further confirming our suggestion of the atomic dispersion of the said metals on ceria.

**NO oxidation performance of M$_1$/CeO$_2$.** We tested these model single-atom materials for NO oxidation. Pt and Pd showed markedly lower NO oxidation activity than Ru (Fig. S6): NO oxidation activity of single atom Pt and Pd materials supported on redox-active supports has not been investigated to date. Typically employed catalysts include Pt and Pd oxide nanoparticles on different supports. We find that both Pt and Pd single atoms have markedly lower activity for NO oxidation, with Pd ions outperforming Pt. 0.5 wt% Ru/ceria sample, in contrast, showed excellent NO oxidation activity in the steam-containing lean $NO/O_2/N_2$ stream (Fig. 1).

The sample shows stable performance with little hysteresis going down, up and then back down in temperature (from 650 ºC to 300 ºC). Activity maximum is observed at ~345 ºC, with ~ 75% conversion of NO. We also tested this sample in the dry NO oxidation (Fig. 1) and did not observe any prominent water influence on the NO oxidation activity. Previously, only 1 study reported the activity of isolated metal atoms (Pt) on alumina for NO oxidation [71], whereas the same authors found that Pd atoms on alumina were inactive [72]. We note that the activity of single-atom Ru, Pd and Pt catalysts on ceria in terms of TOF is ~ an order of magnitude higher than the tabulated activity of Pt atoms and nanoparticles on alumina. Comparison with representative materials in terms of TOF can be found in Table S5. For comparison of NO oxidation activity on supported PGM and non-PGM nanoparticles we refer the readers to the available reviews on this topic [76].

We hypothesized that excellent NO oxidation activity only by single-atom Ru (and not Pt and Pd) is related to the presence of labile active lattice oxygen of ceria and the ability of Ru ions to form ruthenium nitrosyl complexes. If Ru-NO complexes indeed form, then Ru-ceria should be able not to just oxidize NO but also store NO at lower temperatures: this storage is critical during vehicle cold-start and idle operation when the temperatures of exhaust are lower (~100-120 ºC) and no known catalyst can provide NOx removal at this temperature. More specifically, Pd/zeolite formulations can store NOx at low temperatures (~100 ºC) and release them continuously > 180 ºC [7-26]. Pd is expensive and loadings of ~ at least 1-2 wt% are required to achieve optimal NO adsorption.

**NO storage performance of $M_1/CeO_2$.** We, therefore, performed NO adsorption experiments on single-atom M/Ceria materials. Pt and Pd store little NO, consistent with lack of strong bond formation between NO and Pd(II)/Pt(II) on ceria (Fig. S7).

We would like to note that formulations with Pd and Pt nanoparticles on ceria have been considered before for NOx adsorption applications [73-75]. These formulations had high loadings of PGMs (>1 wt%) and were characterized by relatively low NOx storage capacity (~20 μmoles/g), whereas Pd/Zeolite formulations had maximum storage capacity < 180 μmoles/g in the best formulations for 2 wt% Pd/SSZ-13 [8].

0.5 wt% $Ru_1/CeO_2$, however, showed very high NO uptake (Fig. S7, Fig. 2) with full consumption of NO (level ~ 0 ppm) even at 100 ºC. Its performance is better than performance of Pd/SSZ-13 with Pd loading of 2 wt% (Fig. S8). NO/Ru ratio for this sample is ~2.7, showing that there must another avenue of NO storage in addition to Ru-NO complex (discussed further in the text). Hydrothermal aging at 750 ºC in 10%$H_2O/O_2/N_2$ flow under simulated aging conditions does not lead to any appreciable loss of $NO_x$ storage of 0.5 wt% Ru/ceria (Fig. S9), consistent with high stability of $Ru_1/CeO_2$. This is notable considering well-known volatility of $RuO_2$ nanoparticles that typically form at higher Ru loading [68] (see discussion of our EXFAS data) just above ambient temperatures [68]. This hampered use of Ru/Ceria in typical NO reduction or oxidation formulations: those early formulations contained on the order of ~1-2 wt% Ru and thus contained a significant amount of $RuO_2$ nanoparticles (and significantly less isolated Ru sites; see our discussion of EXAFS data). Thus, isolating Ru ions as atomically dispersed species minimizes typical volatilization of extremely volatile $RuO_x$ observed for supported $RuO_x$ nanoparticles [69], and $Ru_1/CeO_2$ represents an excellent NO oxidation catalyst (in the absence of Pt/Pd metals) with outstanding NO storage capacity at cold-start temperatures. We wondered if we could decrease the loading of Ru even further, while maintaining excellent NO adsorption properties and NO oxidation catalysis. We find that even at loading as low as 0.25 wt% Ru, full NO adsorption still can be achieved under simulated cold-start conditions with excellent NO oxidation activity (Fig. 4). The sample shows stable NO adsorption and NO oxidation activity evaluated continuously over 10 cycles (Figs. 4, S10). Furthermore, exposure of 0.25 wt% $Ru_1/CeO_2$ to $SO_2$ did not lead to destruction of NO adsorption and oxidation performance (Fig. S34), highlighting potential of single-atom materials to resist $SO_2$ poisoning typical for all ceria supported oxidation catalysts. Total NO storage of 0.25 wt% $Ru_1/CeO_2$ is ~190 micromoles/gram, exceeding that of the best reported 2 wt% Pd/SSZ-13 materials: however, those Pd/SSZ-13 materials show degradation over cycling in the presence of CO, whereas $Ru_1/CeO_2$ does not. CO oxidation remains stable as well (Fig. S9,S10). This suggests that Ru/ceria materials with low Ru loadings are active CO oxidation catalysts even in the presence of NO and steam (NO is a known poison). For 0.25 wt% Ru/ceria 90% CO conversion is achieved at 200 ºC in the presence of steam and ~200 ppm NO at GHSV 150 L/g*hr.

For all tested samples ~100% of stored NOx is released upon subsequent thermal ramp. This is underscored by the stability of the NO adsorption/desorption within 10 cycles. Another important finding is the NO/Ru ratio is ~2.7 for 0.5 wt% $Ru_1$, ~4.6 for 0.25 wt% $Ru_1$ and ~15 for 0.05 wt% $Ru_1/CeO_2$. (See detailed discussion in the manuscript further; Fig. S30). Since spectroscopy confirms that 1 Ru ion can adsorb 1 NO, spill-over of NO to the ceria surface occurs and is promoted (catalysed) by Ru presence as it does not occur on other noble metals supported on ceria based on the lack of NO storage. NO is initially stored as nitrites [52] on ceria after spill-over as evidenced by DRIFTS spectra in NO flow and the prominent ~1170 $cm^{-1}$ nitrite band [52] (Fig. S16). NO oxidation activity of 750 ºC hydrothermally aged 0.25 wt% $Ru_1/CeO_2$ sample is comparable to the state-of-the-art industrial catalysts with ~1 wt% Pd (and 0.5 wt% Pt) supported on ceria-aluminas (Fig. S21). The TOF (normalized by total precious metal content) for this sample at 350 ºC is ~50 $hr^{-1}$ whereas it is at least ~ 5 times lower for the state-of-the-art commercial catalyst (for which metallic or oxidized nanoparticles are considered to be active sites) tested under similar conditions and having ~ 1 wt% Pd and Pt (Fig. S5).

**Infra-red spectroscopy studies on NO interaction with $Ru_1/CeO_2$.** Ru-containing materials were studied for various catalytic processes [51,52] in the past, yet no spectroscopic investigation of single-atom Ru materials [43-46] was reported. A recent study [50] on catalytic $CO_2$ hydrogenation, reported for 0.5 wt% Ru on ceria that dispersion of Ru nanoparticles into isolated Ru ions changed selectivity of hydrogenation from methane to CO. We, therefore, studied CO and NO adsorption with infra-red spectroscopy on 0.5 wt% Ru/ceria sample. CO adsorption (Figs. S8,S9) on the sample produces no metallic CO bands for Ru and reveals the presence of $Ru(II)(CO)_2$ and $Ru(II)(CO)_3$ complexes on the surface. Adsorption of NO produces a sharp band due to NO interaction with cationic Ru at ~1,850 $cm^{-1}$ (Fig. 3A).

This clearly indicates the formation of a Ru-NO complex, stable even under high vacuum of ~$10^{-8}$ Torr (Fig. 3B).

**Modeling of Ru$_1$/CeO$_2$ and infra-red data.** Recent advances in modeling ceria surface and metal-ceria interactions using state-of-the-art DFT methods can provide a molecular level insight into the precise nature and location of metal ions on ceria surfaces [60-68]. Therefore, we modelled NO complexes of Ru cations adsorbed in different locations on ceria. Five different RuO(NO)/$Ce_{21}O_{42}$ complexes were modelled (Fig. 3, Table S2). The most stable one, e-1O_NO, is obtained after adsorption of NO to the most stable RuO/$Ce_{21}O_{42}$ complex, e-1O (notation of the structures is as in Ref. 63).

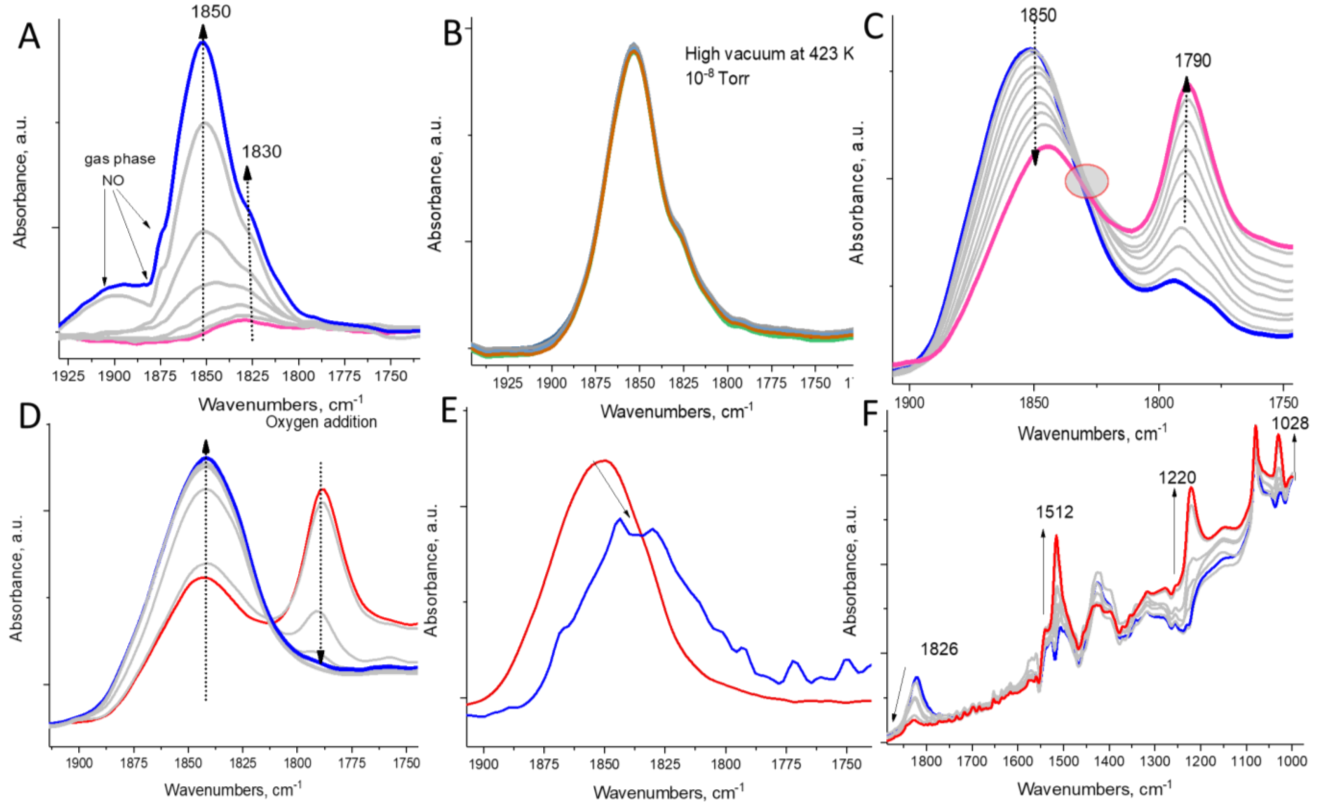

*Figure 3. A. NO adsorption (0.5 Torr equilibrium pressure) at 298 K B. High vacuum after NO adsorption at 423 K . C. Heating Ru-NO from 150 to 220 ºC D. Introducing $O_2$ at 220 ºC after heating Ru-NO E. Water adsorption on Ru-NO complex at 120 ºC F. Ru-NO heated in the presence of $O_2$+$H_2O$ from 120 to 350 ºC: Ru-NO diminishes and chelating nitrates form (bands at 1512, 1220 and 1028 cm$^{-1}$)[53].*

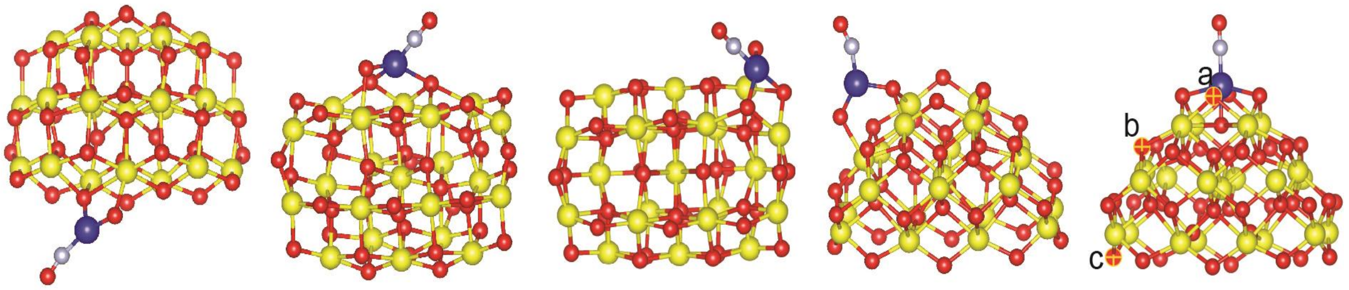

a-1O_NO b-1O_NO c-1O_NO d-1O_NO e-1O_NO

*Figure 4. Optimized RuO(NO)/$Ce_{21}O_{42}$ structures. In the case of e-1O_NO complex with letters are denoted the O centers which are removed in order to obtain RuO(NO)/$Ce_{21}O_{41}$ structures. Color coding of atoms: Ce – yellow, O – red, Ru – dark blue, N – gray. Additional snapshots of the $Ce_{21}O_{42}$ particle and its facets are shown in Fig. S33.*

In this complex, where Ru center is in octahedral coordination at the small (100) facet of the $Ce_{21}O_{42}$ nanoparticle (Fig. S33), NO donates an electron to a $Ce^{4+}$ center, thus $NO^+$ ligand and a $Ce^{3+}$ center are formed, while the formal charge of the Ru remains +2. The other structures modelled are less stable by 1.42-2.91 eV, as the formal charge of Ru is +1, since the unpaired electron is transferred from NO to the Ru center. In the structures a-1O_NO and d-1O_NO, Ru is in triangular planar coordination, interacting with two O centers and the N atom from NO. The lowest N-O vibrational frequencies were calculated for these two structures, 1733 and 1763 cm$^{-1}$. Ru is in square-planar coordination in the structures b-1O_NO and c- 1O_NO, which leads to higher N-O frequencies, 1799 and 1824 cm$^{-1}$. The highest frequency was calculated for the most stable structure, e-1O_NO, 1840 cm$^{-1}$, where Ru is in octahedral coordination (5 O and 1 N). This value is in excellent agreement with the experimental band at 1850 cm$^{-1}$. Thus, FTIR with probe molecule NO combined with state-of-the-art DFT calculations precisely identify location of active isolated $Ru^{+2}$ cations at the small (100) facets of ceria nanoparticles.

Upon temperature increase in the absence of oxygen (Fig. 3C) this band begins to decline with a new band growing at ~ 1790 $cm^{-1}$ and a clear isosbestic point indicating the simple stoichiometric transition of one Ru-NO complex into the other. We suggest that this occurs due to oxygen-vacancy formation in the vicinity of the Ru atom: ON-Ru(vac)Ce. DFT calculations further corroborate this finding. To understand this process, we modeled structures with created O vacancy from $RuO(NO)/Ce_{21}O_{42}$ complexes (Table S2).

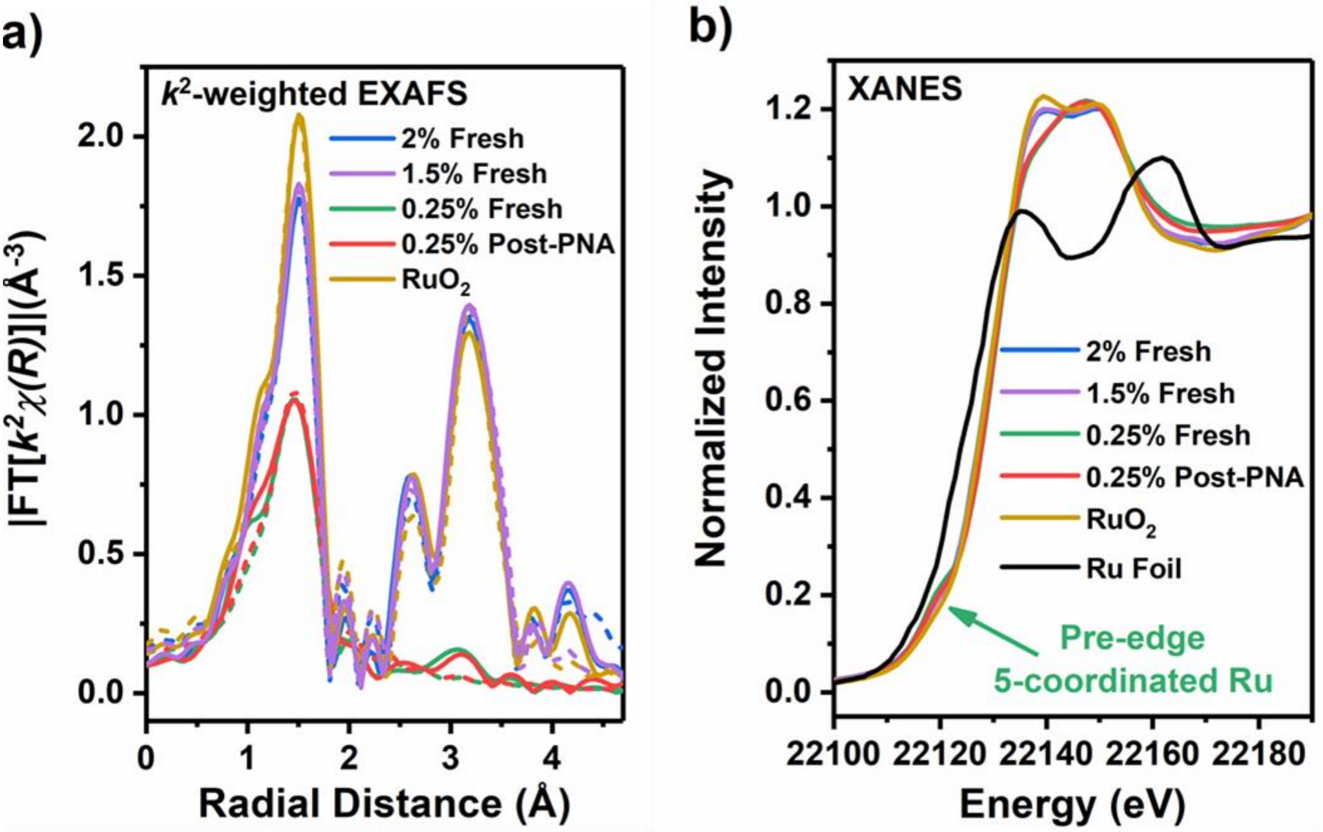

*Figure 5. Ru K-edge XAS results on fresh 2% (blue), 1.5% (purple), 0.25% (green), and post-PNA 0.25% (red) samples. Panel* ***a)*** *shows the EXAFS (R-space magnitude, best fittings shown as dashed curves, fitting parameters listed in Table S4, k-space with fittings shown in Figure S28a). Panel* ***b)*** *shows spectra in the XANES region. Results on $RuO_2$ and Ru foil are presented in yellow and black respectively.*

The most stable structure is e-1O_NO_vac_a, where an O center was removed from the first coordination sphere of the Ru cation. The creation of such O vacancy led to decrease of the N-O vibrational frequency from 1840 to 1788 $cm^{-1}$ in excellent agreement with our experimental results. This is the first direct spectroscopic observation of the formation of an oxygen vacancy on ceria *in the direct vicinity of the metal ion next to ceria*. Further, as soon as we add oxygen to this system, the vacancy is healed, and the NO adsorbed on Ru-O-Ce fully restores, further confirming our suggestion (Fig. 3E). This NO band is robust under high vacuum at 150 °C and does not completely disappear even at 350 °C. In the presence of water, the NO band shifts to lower wavenumbers, the phenomenon that has been previously described for Pd/SSZ-13 and Pd/ZSM-5 and due to co-coordination of water and NO to the same Pd ion [47-49]. We note, for example, that coordination of water to isoelectronic $Rh(I)(CO)_2$ and $Rh(I)(NO)_2$ complexes shifts the CO and NO bands to the lower wavenumbers. Simultaneously, in the presence of $O_2/NO/H_2O$ in the IR cell, infrared spectra emerge after running this under PNA relevant temperatures (~from 120 to 350 °C), showing the decrease of ruthenium nitrosyl complex and increase in chelating nitrate bands on the ceria surface as shown by studies of Hadjiivanov, Vayssilov and co-workers [53]. Thus, ruthenium helps store NO both as a nitrosyl complex and allows $NO_x$ to be stored on the ceria surface due to oxidation ability (as nitrites at low temperature and nitrates at higher temperature in the $O_2$ presence) explaining high NO/Ru ratio which exceeds that of NO/Pd ratio of Pd in zeolites.

**EXAFS studies on $Ru/CeO_2$ with various Ru loadings.** Ru K-edge X-ray absorption spectroscopy (XAS) was performed on selected samples to probe the nuclearity, coordination environment, and electronic state of Ru. Figure 5a shows the $k^2$-weighted EXAFS in *R*-space magnitude (best fittings shown as dashed curves in the same colors). The EXAFS of 2% (blue) and 1.5% (purple) $Ru/CeO_2$ highly resembles that of $RuO_2$ (yellow), with strong scattering between 2 and 4 Å besides first-shell Ru−O scattering at ~1.5 Å. The data can be appropriately modelled by the combination of first-shell Ru−O, second-shell Ru−Ru, Ru−O, third-shell Ru−O, and Ru−O−Ru multiple scattering paths (Table S4) in $RuO_2$ structure. Meanwhile, spectra in the XANES region is presented in Figure 5b, in which the two samples exhibit similar white-line intensity with $RuO_2$, indicating Ru oxidation state close to +4. In addition, there is no pre-edge peak at ~22120 eV in neither samples. This peak represents 1*s* → 4*d* electron transition, which is forbidden on 6-coordinated Ru, but is partially allowed with broken symmetry, i.e., one missing ligand, as 5*p* components are mixed into 4*d* orbitals. Therefore, the absence of this peak suggests that the absolutely majority of Ru on the two samples are 6-coordinated, consistent with the best EXAFS fitting model (Table S4) showing $N$(Ru−O) = 6.4 ± 0.8 and 6.3 ± 0.7, as well as the crystal structure of $RuO_2$. Overall, XAS suggests that on 2% and 1.5% $Ru/CeO_2$, Ru exist mainly as $RuO_2$ particles.

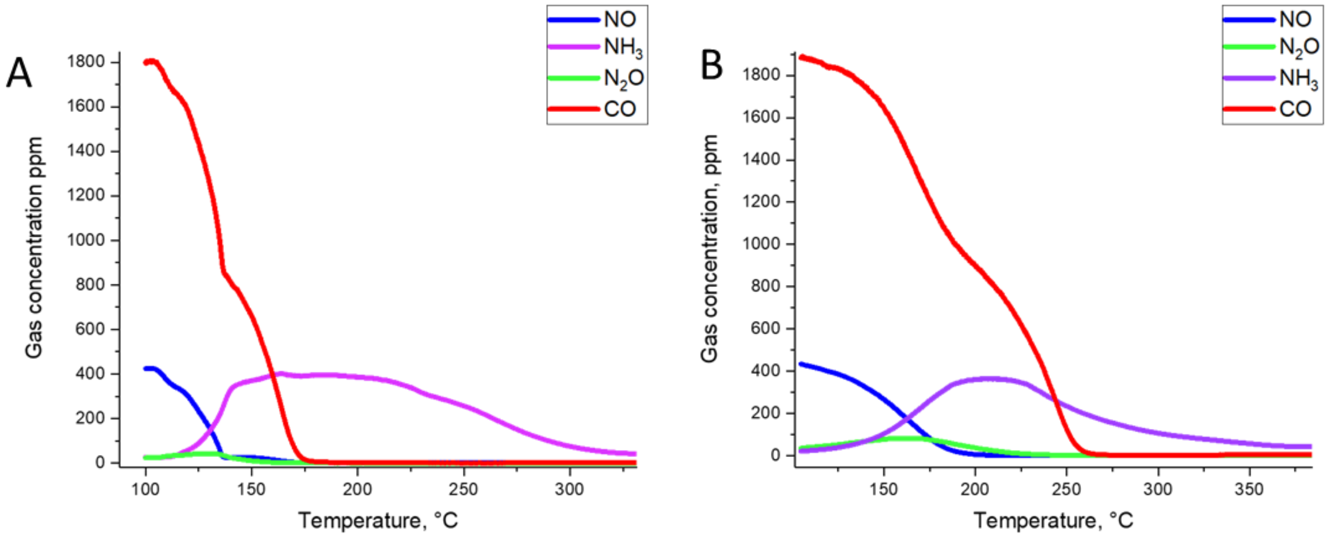

*Figure 6. NO reduction performance of 0.5 wt% $Ru/CeO_2$ (A) and 0.1 wt% $Ru/CeO_2$ (B). 120 mg catalyst, 300 sscm/min total flow, GHSV ~ 150 L/G*hr, 470 ppm NO, 1850 ppm CO, ~3% $H_2O$ balnaced in $N_2$. Performance of 0.5 wt% $Ru/CeO_2$ sample under dry conditions is shown in Fig. S16. Excellent performance of 0.5 and 0.1 wt% Ru/Ceria is comparable to recently reported state-of-the-art catalyst with 1 wt% Pd on Fe-doped ceria [77].*

In contrast, the EXAFS of fresh 0.25% $Ru/CeO_2$ (green) has very low-intensity scattering between 2 and 4 Å. The response of the features in this range to changes in $k$-weight is similar with first-shell Ru−O scattering at ~1.5 Å, and much less sensitive than features in this range in 2%, 1.5% samples and $RuO_2$ which have significant Ru−Ru contribution (Figure S28,S29). This fact indicates that such features in 0.25% $Ru/CeO_2$ have much less high-$k$ contribution than Ru−Ru scattering, i.e., the main contributors are scatterers much lighter than Ru, in this case, O (see Figure S29b for potential paths).

The absence of Ru−Ru contribution to the EXAFS strongly indicates that Ru atoms on 0.25% $Ru/CeO_2$ are atomically dispersed. In the XANES region, the white-line intensity of the sample is between that of $RuO_2$ and Ru foil (black), implying Ru oxidation state between +4 and 0, consistent with Ru(II) from DFT results. Furthermore, 0.25% $Ru/CeO_2$ shows obvious ~22120 eV pre-edge peak, indicating that a significant fraction of Ru are 5-coordinated, aligned well with the best model for its first-shell EXAFS having $N$(Ru−O) = 4.5 ± 0.8 (Table S4), also consistent with DFT results. In fact, when using two first-shell Ru−O paths of different distance in the model, the bond length and coordination number ("2 O" models in Table S4) of both types of Ru−O *perfectly* match structures determined by DFT. We note that after fitting the EXAFS of 0.25% $Ru/CeO_2$ with only first-shell Ru−O, the residual oscillation is mostly in the low-$k$ (< 6 $Å^{-1}$) range (Figure S28a), further confirming that the scattering beyond first-shell has no Ru−Ru contribution. After use in PNA, neither the EXAFS nor the white-line intensity of 0.25% $Ru/CeO_2$ visibly changes (Figure 6, red compared to green), and the EXAFS still has no Ru−Ru contribution (Figures S28a, S29 and Table S4), i.e., Ru remain as atomically dispersed Ru(II) post-PNA. The pre-edge peak in the XANES region diminishes slightly, suggesting that fewer Ru atoms are 5-coordinated, likely a result of residual NO adsorption on Ru. In summary, XAS indicates that Ru on fresh 0.25% $Ru/CeO_2$ are single Ru(II) atoms, many of which are 5-coordinated, and they are stable after PNA. Thus, the coordination environment of Ru on ceria represents a new type of environment not observed for typically employed metal ions on ceria such as Rh, Pd, Pt that are found on step edges and in the square-planar environment of oxygens. That is exemplified by significantly different performance of $Ru_1/CeO_2$ for NO storage and oxidation compared to the typical $M_1/CeO_2$ and $M_{nanoparticle}$/Ceria catalysts that store >10 times less NO and that catalyze NO oxidation only when significant amounts of oxide nanoparticles are present.

Since we discovered there are two mechanistic pathways of NO storage, we put vanishingly small amounts of Ru (0.05 wt%) on ceria and tested NO storage performance. Remarkably, this sample showed facile and excellent NO adsorption under industrially relevant conditions with NOx/Ru ratio approaching 15 (Fig. S30; compare with 1 wt% Ru/Ceria in Fig S31). This, of course, means that $NO_x$ is stored on the ceria surface and the spill-over is facilitated even by the smallest amounts of Ru ions on the surface, revealing a new phenomenon in metal-ceria chemistry to improve interaction of ceria with NO species: this unprecedentedly high ability of Ru ions to function as a shuttle for NOx molecules is believed to be important for various sensing, adsorption and catalytic applications. This also allows us to disentangle the support-related storage and Ru related storage: for 0.25 wt% Ru/ceria material subtracting the baseline storage of NOx on 0.05 wt% Ru/ceria yields approximately ~1.4 molecules of NO per Ru atom (obviously, higher amounts of Ru facilitate even more spill-over of NOx in addition to each Ru atom storing ~ 1 NO molecule).

**Understanding mechanism of NO oxidation on $Ru_1/CeO_2$ using spectroscopy and modelling.** We further investigated NO oxidation mechanism of $Ru_1/CeO_2$ using combined DRIFTS and mass spectrometry. Figs. S15-S20 show *sequential* in-situ DRIFTS and mass spectroscopy experiments that were performed.

We first performed NO adsorption in the DRIFTS flow-through cell, and the result agrees with static IR experiment: upon NO adsorption Ru-NO complex forms and surface nitrites form in great amounts. In the presence of oxygen, surface nitrites turn to surface nitrates at elevated temperatures. Only when the nitrates begin to decompose, mass-spec TPD with in-situ DRIFTS reveals that $NO_2$ begins to form (this holds true for a few continuous IR/TPD MS cycles performed) (Figs S18,S19). We considered the NO oxidation on $RuO/Ce_{21}O_{42}$ complexes (Table S3 and Fig. S27), considering the most stable positions for RuO species on both types of facets (100 and 111) on the $Ce_{21}O_{42}$ nanoparticle, e-1O and c-1O structures, respectively. This process includes four reaction steps: (1) oxidation of Ru species to RuO; (2) adsorption of NO to $RuO/Ce_{21}O_{42}$; (3) NO oxidation to $NO_2$ on Ru, as in the case of c-1O_NO complex the oxidation was considered from the additionally adsorbed in the first reaction step O center, while in the e-1O_NO complex the oxidation was done by an O center from the (100) facet; (4) $NO_2$ desorption from $Ru/Ce_{21}O_{42}$. The first two adsorption steps are strongly exothermic, while the oxidation and desorption are strongly endothermic. The rate-limiting step appears to be the NO oxidation, as the barriers are as high as 182 and 249 kJ/mol, respectively, on c-1O and e-1O sites. However, if all contributions to the enthalpy as well as the entropy are taken into account at temperature of 623 K, the corresponding Gibbs free barriers become 154 and 200 kJ/mol. The former barrier seems to be operative at 623 K, as the calculated kinetic constant is 1.58 $s^{-1}$ (pre-exponential factor of the Eyring equation was taken to be 1) which corresponds to a half-life T½ of ~0.44 sec. The $NO_2$ desorption is strongly endothermic, but when the entropy contribution is considered the endothermicity of the process is reduced by ~150 kJ/mol, as in the case of e-1O complex it becomes even exothermic. This corresponds very well with our DRIFTS/Mass-spec data showing that NO association with interfacial Ru-O-Ce oxygen as well as nitrate decomposition steps are the legitimate pathways of $NO_2$ formation. The real rate constant at 623 K corresponds is ~0.015 $s^{-1}$ per Ru site (~50 $hr^{-1}$). The significantly lower number actually also suggests that not all sites participate in catalysis. Furthermore, it exceeds the TOF estimated for the most effective bimetallic and mono-metallic Pt and PtPd catalysts by at least ~5 times [68]. For active catalytic formulations tested under similar industrially relevant conditions, normalization of the TOF frequencies in the desired temperature range per total precious metal amount yields TOF frequencies on the order of ~6 $hr^{-1}$. It is important to note that the industrial formulations always include significant amounts of Pd and Pt (total loading ~1.5-2 wt% typically). Therefore, Ru-O-Ce sites of single-atom Ru/ceria catalysts are very active for NO oxidation. However, the corresponding single-atom Pt(Pd)-O-Ce are poorer NO (and CO, for Pt [28-31]) oxidation catalysts due to inability of Pt and Pd to form a stable Metal-NO bond that would ensure coverage of NO when the interfacial O removal from M-O-Ce sites becomes favourable, as well as a spill-over of NO species onto the ceria support as nitrates. Thus, $Ru_1/CeO_2$ stands out as the only known ceria-supported material able to form thermally stable Ru-NO complexes.

**Activity of $Ru_1/CeO_2$ in NO reduction by carbon monoxide.** To confirm the versatility of Ru/ceria materials for NOx abatement catalysis, we now turn our attention to another challenging reaction for gasoline engines called NO reduction. TWC materials should perform catalytic removal of NOx in the presence of CO and water vapor under stoichiometric conditions [39-42]. We recently discovered that isolated Rh(I) ions on ceria can perform low temperature NO reduction by CO [42] effectively. We, therefore, wondered if isolated Ru(II) ions could also perform NO reduction by CO [69-71]. 0.5 wt% Ru/ceria sample is excellent for NO reduction by CO under dry conditions [77]. Addition of water to the stream, in fact, does not lead to activity deterioration (Fig. 6, Fig.S21): in this case ammonia production is observed in significant amounts, due to Ru/ceria being an excellent water-gas-shift catalyst [42]. Decreasing Ru loading to 0.1 wt% also produces an active NO reduction catalyst, with excellent activity and full NO conversion ~185 °C (Fig. 6). Thus, $Ru_1/CeO_2$ is an active catalyst for NO reduction by CO even at low Ru loading. TOF per Ru atoms ~ 370 $hr^{-1}$ at 185 °C. In our recent paper [42] we showed the first example of single atom Rh ceria-supported catalyst for NO reduction by CO, very active at low temperatures. Under similar GHSV and testing conditions, Rh single atoms were active catalysts with TOF ~300 $hr^{-1}$ at ~130 ºC. Although Ru(II) ions are marginally less active than Rh, the impressive catalytic performance is still achieved at low temperature with a significantly cheaper metal. In fact, its performance is comparable with recent reports for state-of-the-art 1wt% Pd catalyst on Fe-doped ceria [77] but on undoped ceria with less PGM (2 to 10 times) and significantly less expensive PGM. Based on our preliminary data [42], we previously suggested a possible catalytic mechanism for $Rh_1/CeO_2$.

The mechanistic aspects of NO reduction by CO have always been elusive because the typical materials used for this reaction contain poorly defined structures (nanoparticles): this made direct correlation of reactivity to structure for NO reduction very problematic. With well-defined single Ru(II) ions on ceria that are present as uniform isolated sites on the redox active surface, we have a unique opportunity to identify the mechanism of NO reduction by CO using in-situ and modulation-excitation infrared spectroscopy under the real flow-through conditions.

**Pinpointing the mechanism of NO reduction by CO on $Ru_1/CeO_2$.** In order to do so, we employed modulation-excitation DRIFTS approach [78-80] in our infra-red measurements: in short, at a temperature where (NO+CO) conversion occurs (150 °C), NO or CO flow pulses were applied to the system in antiphase for 3 consecutive cycles. The bands that appear/disappear in antiphase during these treatments indicate the appearance/consumption of the true catalytically active intermediates. Additionally, we performed in-situ DRIFTS with (NO+CO) flow at the same temperature (Figs 7, S22-S25).

During NO flow (~500 ppm) at 150 °C Ru-NO band at ~1850 $cm^{-1}$ appears, as well as nitrite bands associated with ceria at ~1160 $cm^{-1}$. NO was then stopped, and CO flow started (2,500 ppm) (Fig. 7). Very notable changes were observed: nitrite band quickly decreased, simultaneously, Ce-O-Ru-NO band (1860 $cm^{-1}$) decreased with the concomitant evolution of the Ce-vacancy-Ru-NO band (1790 $cm^{-1}$). Furthermore, the carbonate bands, easily attributable to poly- and mono-dentate carbonates, appeared (due to $CO_2$ evolution; some of which re-adsorbs on the surface at 150 °C).

We then followed with NO treatment: NO treatment leads to the fast restoration of the Ru-NO band with the simultaneous healing of the oxygen vacancy; at the same time nitrite bands re-appears at 1160 $cm^{-1}$. Repetition of these NO-CO modulation-excitation cycles 3 times, allows to observe the phases that appear/disappear (respond dynamically during each cycle; Figs16-S20). The ones that are in anti-phase correspond to the active catalytic intermediates of the NO reduction by CO: indeed, during CO reduction: nitrites bands and Ru-NO bands are consumed with the formation of the oxygen vacancy between Ru(vacancy)Ce and $CO_2$ (carbonates). Treatment with NO, leads to re-filling of the oxygen vacancy with oxygen from NO and restoration of nitrite bands. We previously suggested based on ex-situ measurements that for $Rh_1/CeO_2$ CO reduces Rh(III) to Rh(I) (which we suggested to be the rate-limiting step of this reaction) with the following re-oxidation of Rh(I) with NO to Rh(III). Now, we show generally that we observe similar chemistry in-situ: but in this case, we prove the importance and direct participation of the oxygen vacancy between Ru and Ce in the catalysis: this vacancy is created by the process (1-5):

(1) CO-Ru-O-Ce → $CO_2$ + Ru (vac) Ce
(2) Ru (vac) Ce + 2 NO → NO-Ru (vac) Ce-NO → $Ru(N_2O_2)Ce$ → Ru-O-Ce + $N_2O$

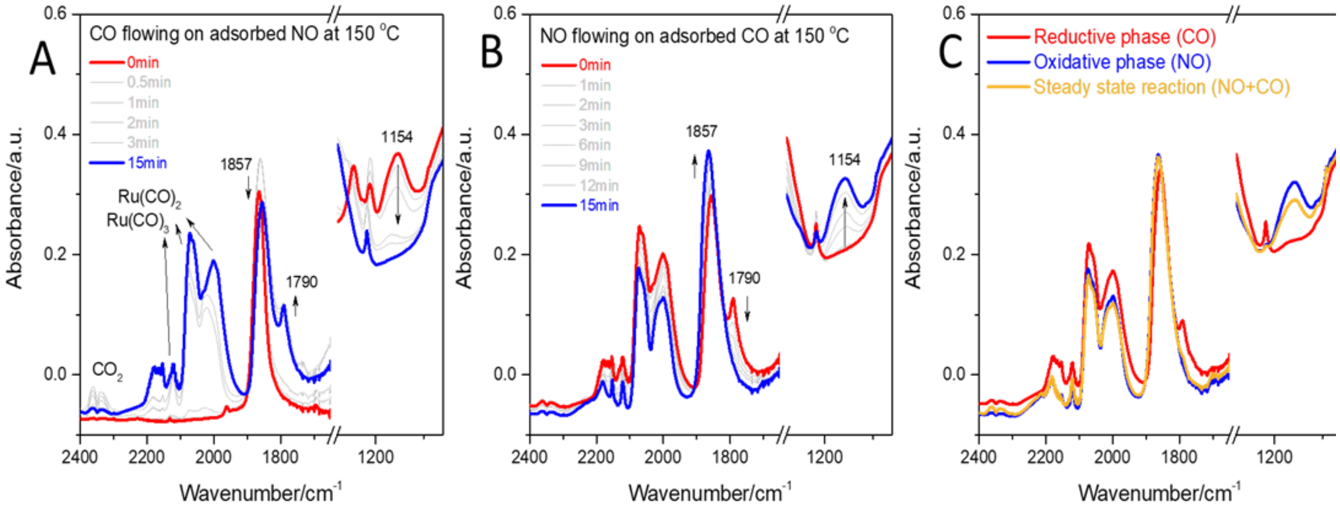

*Figure 7. In-situ DRIFTS on 0.25 wt% $Ru_1/CeO_2$. A. Exposure to CO (2,500 ppm) of NO-saturated sample (saturated with 500 ppm NO flow for 30 minutes, then purged with He at 150 $^{0}$C before exposure to CO) B. Subsequent exposure to NO flow after CO at 150 $^{0}$C. C. Comparison of the $Ru_1/CeO_2$ during exposure to 2,500 ppm CO in the flow („reductive phase“), 500 ppm exposure to NO in the flow („oxidative phase“), and (500 pppm NO + 2,5000 ppm CO) exposure in the flow (steady state reaction; in the DRIFTS cell NO conversion ~ 30% under these conditions) at 150 $^{0}$C.*

(3) NO-Ru-O-Ce → Ru (vac) Ce-$NO_2$
(4) CO+ Ru (vac) Ce-$NO_2$ → CO-Ru Ce-$NO_2$ → $CO_2$ + Ru(vac)Ce-NO + NO → Ru ($N_2O_2$) Ce → Ru-O-Ce + $N_2O$
(5) Ru(vac)Ce + $N_2O$ → O=N=N-Ru(vac)Ce → $N_2$ + Ru-O-Ce

The observation of the surface species during (NO+CO) flow over Ru/ceria sample in the DRIFTS cell (~30% NO conversion based on Mass-Spec data), and comparison with the states during NO and CO flows (Fig. 7), allows to conclude that during the reaction the surface remains mostly "oxidized". This can be rationalized by the fact that the rate-limiting step of NO reduction is the removal of O between Ru-O-Ce by CO with the formation of $CO_2$: the subsequent steps (re-filling of the oxygen vacancy by NO) occur much faster, and during NO+CO flow we find basically mostly oxidized surface. We emphasized earlier in the manuscript the remarkable lability of oxygens of ceria in $Ru_1/CeO_2$. That holds even for ultra-low Ru loadings of 0.05 wt% which we further prove with XPS (Fig. S32; presence of only 0.05 wt% Ru is sufficient to observe the greatly increased surface reducibility of Ce after CO or $H_2$ treatments under mild conditions).

To further show the benefit of ultra-low Ru amounts on TWC, we performed NO reduction catalysis on 0.2 wt% Rh materials supported on ceria in the presence and absence of 0.05 wt% Ru (Fig. S35). We tested these catalysts fresh and after harsh aging (950 $^{0}$C, 10% $H_2O/N_2$ flow, 5 hours). Addition of such small amount of Ru, resulted in shift of NO and CO conversion curves to lower temperatures both for fresh and aged catalysts by at least 25 $^{0}$C, highlighting benefits of ultra-low Ru amounts for typical Rh TWC catalyst.

Thus, the in-situ dynamic NO/CO experiment allowed us to clarify the mechanism as well as slow/fast steps of NO/CO reaction on atomically dispersed metal catalysts for the first time.

**Conclusions.** In summary, we show brand new aspects of adsorptive and catalytic chemistry of ceria on the basis of well-defined $Ru_1/CeO_2$ catalysts. They show promising performance for challenging $NO_x$ pollutant abatement even at low metal loadings. We elucidate the location of active Ru(II) cations on the surface of ceria and provide molecular level understanding of the mechanism of NO oxidation, low-temperature NO storage and NO reduction by CO on these materials, paving the way for further developments in the important field of ceria-supported noble metals.

### Supporting Information

The Supporting Information contains the detailed description of materials and methods, HAADF-STEM images and corresponding EDS maps, adsorption and catalytic data, DFT optimized structures and DFT data, EXAFS analysis data, infrared spectroscopy data.

## Acknowledgements

The research at PNNL was supported by the U.S. Department of Energy, Energy Efficiency and Renewable Energy, Vehicle Technology Office. Experiments were conducted in the Environmental Molecular Sciences Laboratory (EMSL), a national scientific user facility sponsored by the Department of Energy's Office of Biological and Environmental Research at Pacific Northwest National Laboratory (PNNL). PNNL is a multi-program national laboratory operated for the DOE by Battelle Memorial Institute under Contract DE-AC06-76RL01830. We acknowledge the support of CLEERS (Crosscut Lean Exhaust Emissions Reduction Simulations). CLEERS is an initiative funded by the U.S. Department of Energy (DOE) Vehicle Technologies Office to support the development of accurate tools for use in the design, calibration, and control of next generation engine/emissions control systems that maximize efficiency while complying with emissions regulations. HAA gratefully acknowledges the support by Bulgarian National Science Fund (project DN-19/2). GNV acknowledges the support of the project EXTREME, funded by the Bulgarian Ministry of Education and Science, D01-76/30.03.2021 through the programme "European Scientific Networks". Computational resources are provided by Avitohol supercomputer, supported by Bulgarian Ministry of Education and Science via National Roadmap for Research Infrastructures.

The previous version of this paper was uploaded on the pre-print server ChemRxiv on July 23rd 2020:

DOI: 10.26434/chemrxiv.12692264.v1

*Corresponding authors.

**Conflict of interest**

No conflicts to declare.

**TOC**

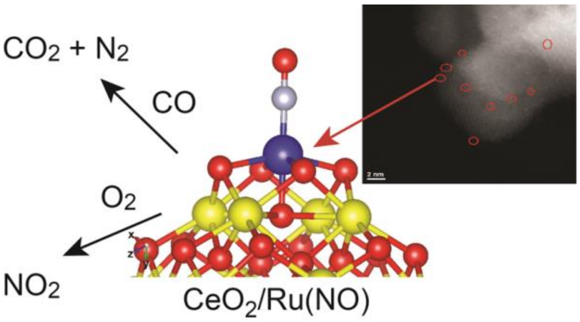

**References**

(1) S. T. Holgate, 'Every breath we take: the lifelong impact of air pollution' – a call for action, Clinical Medicine, 2017, 17, 8–12.
(2) N. R. Jaegers, J. K. Lai, Y. He, E. Walter, D. A. Dixon, M. Vasiliu, Y. Chen, C. M. Wang, M. Y. Hu, K. T. Mueller, I. E. Wachs, Y. Wang, J. Z. Hu, Mechanism by which Tungsten Oxide Promotes the Activity of Supported V2O5/TiO2 Catalysts for NOX Abatement: Structural Effects Revealed by 51V MAS NMR Spectroscopy, Angew. Chem., Int. Ed., 2019, 131, 12739–12746.
(3) J-H. Kwak, R. G. Tonkyn, D. H. Kim, J. Szanyi, C. Peden, J. Catal., Excellent activity and selectivity of Cu-SSZ-13 in the selective catalytic reduction of NOx with NH3, J. Catal. 2010, 275, 187-190.
(4) I. Bull, A. Moini, G. Koermer, J. Patchett, W. Jaglowski, S. Roth, Zeolite catalyst with improved NOX reduction in SCR, US Patent US20070134146A1, 2010.
(5) S. I. Zones, Zeolite SSZ-13 and its method of preparation, US Patent 4 544 538, 1985.
(6) T. Seiyama, T. Arakawa, T. Matsuda, N. Yamazoe, Y. Takita, Catalytic reduction of nitric oxide with ammonia over metal ion-exchanged Y zeolites, Chem. Lett. 1975, 781-784.
(7) H.-Y. Chen, J. E. Collier, D. Liu, L. Mantarosie, D. Durán- Martín, D.; V. Novák, R. Rajaram, D. Thompsett, Low Temperature NO Storage of Zeolite Supported Pd for Low Temperature Diesel Engine Emission Control, Catal. Lett. 2016, 146, 1706–1711.
(8) K. Khivantsev, N. R. Jaegers, L. Kovarik, J. C. Hanson, F. F. Tao, Y. Tang, X. Zhang, I. Koleva, H. A. Aleksandrov, G. N. Vayssilov, Y. Wang, F. Gao, J. Szanyi, Achieving atomic dispersion of highly loaded transition metals in small-pore zeolite SSZ-13, Angew. Chem. 2018, 130, 16914–16919.
(9) Khivantsev, K.; Jaegers, N. R.; Kovarik, L.; Prodinger, S.; Derewinski, M. A.; Wang, Y.; Gao, F.; Szanyi, J. Palladium/Beta zeolite passive NOx adsorbers (PNA): Clarification of PNA chemistry and the effects of CO and zeolite crystallite size on PNA performance, Appl. Catal. A. Gen. 2019, 569, 141–148.
(10) Khivantsev, K.; Jaegers, N. R.; Koleva, I. Z.; Aleksandrov, H. A.; Kovarik, L.; Engelhard, M.; Gao, F.; Wang, Y.; Vayssilov, G. N.; Szanyi, J. Stabilization of Super Electrophilic Pd+2 Cations in Small-Pore SSZ-13 Zeolite, J. Phys. Chem. C 2020, 124, 309–321.
(11) K. Khivantsev, F. Gao, L. Kovarik, Y. Wang, J. Szanyi, Molecular level understanding of how oxygen and carbon monoxide improve NO x storage in palladium/SSZ-13 passive NO x adsorbers: The role of NO+ and Pd (II)(CO)(NO) species, J. Phys. Chem. C 2018, 122, 10820–10827.
(12) M. Moliner, A. Corma, From metal-supported oxides to well-defined metal site zeolites: the next generation of passive NOx adsorbers for low-temperature control of emissions from diesel engines, React. Chem. Eng. 2019, 4, 223–234.
(13) K. Khivantsev, N. R. Jaegers, L. Kovarik, J. Z. Hu, F. Gao, Y. Wang, J. Szanyi, Palladium/zeolite low temperature passive NOx adsorbers (PNA): structure-adsorption property relationships for hydrothermally aged PNA materials, Emiss. Control Sci. Technol. 2020, 6, 126–138.
(14) E. Bello, V. J. Margarit, E. M. Gallego, F. Schuetze, C. Hengst , A. Corma, M. Moliner, Deactivation and regeneration studies on Pd-containing medium pore zeolites as passive NOx adsorbers (PNAs) in cold-start applications, Microporous and Mesoporous Materials 302 (2020) 110222.
(15) Khivantsev, K.; Jaegers, N. R.; Kovarik, L.; Wang, M.; Hu, J. Z.; Wang, Y.; Derewinski, M. A.; Szanyi, J. The Superior Hydrothermal Stability of Pd/SSZ-39 in Low Temperature Passive NOx Adsorption (PNA) and Methane Combustion, Appl. Catal., B 2021, 280, 119449.
(16) R. Rajaram, H.-Y. Chen, D. Liu, Passive NOx adsorber, US Patent US20150158019A1, 2015.
(17) I. Song, K. Khivantsev, Y. Wu, M. Bowden, Y. Wang, Janos Szanyi, Unusual water-assisted NO adsorption over Pd/FER calcined at high temperatures: The effect of cation migration, Applied Catalysis B: Environmental, 2022, 318, 121810.
(18) I. Song, K. Khivantsev, Y. Wang, J. Szanyi, Elucidating the Role of CO in the NO Storage Mechanism on Pd/SSZ-13 with in Situ DRIFTS, J. Phys. Chem. C 2022, 126, 3, 1439–1449.
(19) K. Khivantsev, J. Szanyi, N.R. Jaegers, L. Kovarik, F. Gao, Y. Wang, High-capacity, low-temperature, passive NOx and CO adsorbers and methods for making same, US Patent 11,071,966, 2021.
(20) J. Lee, T. H. Lim, E. Lee, D. H. Kim, Promoting the Methane Oxidation on Pd/CeO2 Catalyst by Increasing the Surface Oxygen

Mobility via Defect Engineering, ChemCatChem 2021, 13, 3706-3712

(21) J. Lee, Y. Kim, S. Hwang, E. Lee, H. Lee, C.H. Kim, D.H. Kim, Deactivation of Pd/Zeolites passive NOx adsorber induced by NO and H2O: Comparative study of Pd/ZSM-5 and Pd/SSZ-13, Catal. Today 2021, 360, 350-355.

(22) I. Heo, Y. W. You, J. H. Lee, S. J. Schmieg, D. Y. Yoon, C. H. Kim, Urealess NOx Reduction by Carbon Monoxide in Simulated Lean-Burn Exhausts , Environ. Sci. Technol. 2020, 54, 13, 8344–8351.

(23) Ryou, Y. S.; Lee, J.; Cho, S. J.; Lee, H.; Kim, C. H.; Kim, D. Activation of Pd/SSZ-13 catalyst by hydrothermal aging treatment in passive NO adsorption performance at low temperature for cold start application, Appl. Catal. B Environ. 2017, 212, 140–149.

(24) Ryou, Y. S.; Lee, J.; Lee, H.; Kim, C. H.; Kim, D. H., Effect of various activation conditions on the low temperature NO adsorption performance of Pd/SSZ-13 passive NOx adsorber , Comparative study of the mobility of Pd species in SSZ-13 and ZSM-5, and its implication for their activity as passive NOx adsorbers (PNAs) after hydro-thermal aging, Catal. Today 2019, 320, 175–180.

(25) Lee, J.; Ryou, Y.; Hwang, S.; Kim, Y.; Cho, S. J.; Lee, H.; Kim, C. H.; Kim, D. H., Comparative study of the mobility of Pd species in SSZ-13 and ZSM-5, and its implication for their activity as passive NOx adsorbers (PNAs) after hydro-thermal aging , Catal. Sci. Technol. 2019, 9 (1), 163–173.

(26) Kim, Y.; Hwang, S.; Lee, J.; Ryou, Y. S.; Lee, H.; Kim, C. H.; Kim, D. H. Comparison of NOx Adsorption/Desorption Behaviors over Pd/CeO2 and Pd/SSZ-13 as Passive NOx Adsorbers for Cold Start Application, Emiss. Control Sci. Technol. 2019, 5 (2), 172–182.

(27) Khivantsev, K.; Wei, X.; Kovarik, L.; Jaegers, N. R.; Walter, E. D.; Tran, P.; Wang, Y.; Szanyi, J. Palladium/Ferrierite versus Palladium/SSZ-13 Passive NOx Adsorbers: Adsorbate-Controlled Location of Atomically Dispersed Palladium(II) in Ferrierite Determines High Activity and Stability. Angew. Chem., Int. Ed. 2022, 61, e202107554.

(28) Pereira-Hernandez, X. I.; DelaRiva, A.; Kunwar, D.; Xiong, H.; Sudduth, B.; Engelhard, M.; Kovarik, L.; Murayev, V.; Hensen, E.; Wang, Y.; Datye, A. K. Tuning Pt-CeO2 interactions by high-temperature vapor-phase synthesis for improved reducibility of lattice oxygen, Nat. Commun. 2019, 10 (1), 1358.

(29) Datye, A.; Wang, Y. Atom trapping: a novel approach to generate thermally stable and regenerable single-atom catalysts, Natl. Sci. Rev. 2018, 5, 630–632.

(30) Jones, J.; Xiong, H.; DeLaRiva, A. T.; Peterson, E. J.; Pham, H.; Challa, S. R.; Qi, G.; Oh, S.; Wiebenga, M. H.; Pereira Hernandez, X. I.; Wang, Y.; Datye, A. K. Thermally stable single-atom platinum-on-ceria catalysts via atom trapping, Science 2016, 353, 150−154.

(31) Nie, L.; Mei, D.; Xiong, H.; Peng, B.; Ren, Z.; Hernandez, X. I. P.; DeLaRiva, A.; Wang, M.; Engelhard, M. H.; Kovarik, L.; Datye, A. K.; Wang, Y., Activation of surface lattice oxygen in single-atom Pt/CeO2 for low-temperature CO oxidation, Science 2017, 358, 1419.

(32) Twigg, M.V., Haren Gandhi 1941-2010: Contributions to the Development and Implementation of Catalytic Emissions Control Systems. Platinum Metals Review, 2011, 55, 43-53.

(33) W. Martienssen, H. Warlimont, Springer Handbook of Condensed Matter and Materials Data, Springer, 2006.

(34) M. Koebel, M. Elsener, M. Kleemann, Urea-SCR: a promising technique to reduce NOx emissions from automotive diesel engines, Catal. Today 2000, 59, 335.

(35) N. Takahashi et al., The new concept 3-way catalyst for automotive lean-burn engine: NOx storage and reduction catalyst, Catal. Today 1996, 27, 63.

(36) M. Koebel, G. Madia, M. Elsener, Selective catalytic reduction of NO and NO2 at low temperatures, Catal. Today 2002, 73, 239.

(37) P. Bourges, S. Lunati, G. Mabilon, N20 and NO2formation during NO reduction on precious metal catalysts, Catalysis And Automotive Pollution Control IV 116, 213 (1998)

(38) C. H. Kim, G. Qi, K. Dahlberg, W. Li, N2O and NO2 formation during NO reduction on precious metal catalysts, Science, 2010, 327, 1624-1627.

(39) Harrison, B, Diwell, AF, Hallett, C. Promoting Platinum Metals by Ceria, Platin. Metal. Rev. 1988, 32, 73–83.

(40) Taylor, K. Catal. Rev.: Sci. Eng. Nitric Oxide Catalysis in Automotive Exhaust Systems, 1993, 35, 457−481.

(41) Granger, P.; Parvulescu, V. I. Catalytic NOx Abatement Systems for Mobile Sources, Chem. Rev. 2011, 111, 5, 3155–3207.

(42) K. Khivantsev, C. Vargas, J. Tian, L. Kovarik, N. R. Jaegers, J. Szanyi, Y. Wang, Economizing on Precious Metals in Three-Way Catalysts: Thermally Stable and Highly Active Single-Atom Rhodium on Ceria for NO Abatement under Dry and Industrially Relevant Conditions, Angew. Chem. 2021, 133, 395-402.

(43) Hadjiivanov, K.; Lavalley, J.-C.; Lamotte, J.; Mauge, F.; SaintJust, J.; Che, M. FTIR Study of CO Interaction with Ru/TiO2Catalysts J. Catal. 1998, 176, 415.

(44) H. Miessner, Surface Chemistry in a Zeolite Matrix. Well-Defined Dinitrogen Complexes of Rhodium Supported on Dealuminated Y Zeolite, J. Am. Chem. Soc. 1994, 116, 11522-11530.

(45) Miessner, H.; Richter, K. Well-defined carbonyl and dinitrogen complexes of ruthenium supported on dealuminated Y zeolite. Analogies and differences to the homogeneous case, J. Mol. Catal. A-Chem. 1999, 146, 107-115.

(46) H. Kim, S. Yang, Y. H. Lim, J. M. Ha, D. H. Kim, Upgrading bio-oil model compound over bifunctional Ru/HZSM-5 catalysts in biphasic system: Complete hydrodeoxygenation of vanillin, Journal of Hazardous Materials 423, 126525.

(47) Chakarova K, Ivanova E, Hadjiivanov K, Klissurski D, Knozinger H. Co-ordination chemistry of palladium cations in Pd-H-ZSM-5, Phys. Chem. Chem. Phys. 2004, 6, 3702.

(48) J. Lee, J. Kim, Y. Kim, S. Hwang, H. Lee, C. H. Kim, D. H. Kim, Improving NOx storage and CO oxidation abilities of Pd/SSZ-13 by increasing its hydrophobicity, Appl. Catal. B: Env. 2020, 277, 119190.

(49) K. Khivantsev, Selective Synthesis and Characterization of Single-Site HY Zeolite-Supported Rhodium Complexes and Their Use as Catalysts for Ethylene Hydrogenation and Dimerization, University of South Carolina (2015) Ph.D. Thesis (accessed 2022-11-25)

(50) Aitbekova, A.; Wu, L.; Wrasman, C. J.; Boubnov, A.; Hoffman, A. S.; Goodman, E. D.; Bare, S. R.; Cargnello, M. Low-Temperature Restructuring of CeO$_2$-Supported Ru Nanoparticles Determines Selectivity in CO2 Catalytic Reduction. J. Am. Chem. Soc. 2018, 140, 42, 13736–13745.

(51) A.R. Derk, G.M. Moore, S. Sharma, E.W. McFarland, H Metiu, Catalytic dry reforming of methane on ruthenium-doped ceria and ruthenium supported on ceria, Top. Catal. 57, 118–124 (2014).

(52) D. Chester, A. R. Derk, S. Sharma, H. Metiu, E. W. McFarland, Catal. Sci. Technol., CO2 methanation by Ru-doped ceria: the role of the oxidation state of the surface, 2015, 5, 1783-1791.

(53) Mihaylov, M. Y.; Zdravkova, V. R.; Ivanova, E. Z.; Aleksandrov, H. A.; Petkov, P. St.; Vayssilov, G. N.; Hadjiivanov, K. I. Infrared spectra of surface nitrates: Revision of the current opinions based on the case study of ceria. J. Catal. 2021, 394, 245-258.

(54) J. P. Perdew, J. A. Chevary, S. H. Vosko, K. A. Jackson, M. R. Pederson, D. J. Singh, C. Fiolhais, Atoms, molecules, solids, and surfaces: Applications of the generalized gradient approximation for exchange and correlation, Phys. Rev. B, 1992, 46, 6671-6687;

(55) G. Kresse and J. Hafner, Ab initio molecular dynamics for liquid metals, Phys. Rev. B, 1993, 47, 558-561.

(56) Version VASP.4.9; http://cms.mpi.univie.ac.at/vasp (accessed 2022-11-25).

(57) G. Kresse, D. Joubert, From ultrasoft pseudopotentials to the projector augmented-wave method, Phys. Rev. B, 1999, 59, 1758-1775.

(58) V. I. Anisimov, F. Aryasetiawan, A. I. Lichtenstein, First-principles calculations of the electronic structure and spectra of strongly correlated systems: the LDA+ U method, J. Phys.: Condens. Matter, 1997, 9, 767-808.

(59) S. L. Dudarev, G. A. Botton, S. Y. Savrasov, C. J. Humphreys, A. P. Sutton, Electron-Energy-Loss Spectra and the Structural Stability of Nickel Oxide: An LSDA+U Study, Phys. Rev. B, 1998, 57, 1505-1509.

(60) C. Loschen, J. Carrasco, K. M. Neyman, F. Illas, First-principles LDA+U and GGA+U study of cerium oxides, Phys. Rev. B, 2007, 75, 035115.

(61) A. Migani, G. N. Vayssilov, S. T. Bromley, F. Illas, K. M. Neyman, Greatly facilitated oxygen vacancy formation in ceria, Chem. Commun., 2010, 46, 5936-5938.

(62) A. Migani, G. N. Vayssilov, S. T. Bromley, F. Illas, K. M. Neyman, J. Mater. Chem., Dramatic reduction of the oxygen vacancy formation energy in ceria particles: a possible key to their remarkable reactivity at the nanoscale, 2010, 20, 10535-10546.

(63) H. A. Aleksandrov, K. M. Neyman, G. N. Vayssilov, The structure and stability of reduced and oxidized mononuclear platinum species on nanostructured ceria from density functional modelling, Phys. Chem. Chem. Phys. 2015, 17, 14551–14560.

(64) H.A. Aleksandrov, K.M. Neyman, K.I. Hadjiivanov, G.N. Vayssilov, Can the state of platinum species be unambiguously determined by the stretching frequency of an adsorbed CO probe molecule? Phys. Chem. Chem. Phys. 2016 18 (32), 22108-22121.

(65) I.Z. Koleva, H.A. Aleksandrov, G.N. Vayssilov, Decomposition behavior of platinum clusters supported on ceria and γ-alumina in the presence of carbon monoxide, Catalysis Science & Technology, 2017 7 (3), 734-742

(66) G. N. Vayssilov, Y. Lykhach, A. Migani, T. Staudt, G. P. Petrova, N. Tsud, T. Skála, A. Bruix, F. Illas, K. C. Prince, K. M. Neyman, J. Libuda, Support nanostructure boosts oxygen transfer to catalytically active platinum nanoparticles, Nature materials, 2011, 10 (4), 310-315.

(67) J. Lee, Y. S. Ryou, X. Chan, T. J. Kim, D. H. Kim, How Pt Interacts with CeO2 under the Reducing and Oxidizing Environments at Elevated Temperature: The Origin of Improved Thermal Stability of Pt/CeO2 Compared to CeO2, J. Phys. Chem. C 2016, 120 (45), 25870-25879.

(68) R. Alcala, A. DeLaRiva, E. J. Peterson, A. Benavidez, C. Garcia-Vargas, A. Benavidez, D. Jiang, X. I. Pereira-Hernández, H. H. Brongersma, R. Veen, J. Staněk, J. T. Miller, Y. Wang, A. Datye, Atomically Dispersed Dopants for Stabilizing Ceria Surface Area, Appl. Catal. B Env. 2021, 284, 119722

(69) R.L.Klimisch, J.G.Larson, The Catalytic Chemistry of Nitrogen Oxides, Plenum Press, New York (1975).

(70) J. H. Kim, S. Yoon, D. S. Baek, J. Kim, J. Kim, K. An, S. H. Joo, Boosting Thermal Stability of Volatile Os Catalysts by Downsizing to Atomically Dispersed Species, JACS Au 2022, 2, 8, 1811–1817.

(71) C. K. Narula, L. F. Allard, G. M. Stocks, M. Moses-DeBusk, Remarkable NO oxidation on single supported platinum atoms, Sci. Rep. 2014, 4, 7238.

(72) Narula, C.K., Allard, L.F., Moses-DeBusk, M. *et al.* Single Pd Atoms on θ-$Al_2O_3$ (010) Surface do not Catalyze NO Oxidation. *Sci Rep 2013,* **7**, 560.

(73) A. Toso, M. Danielis, C. de Leitenburg, M. Boaro, A. Trovarelli, S. Collussi, Key Properties and Parameters of Pd/CeO2 Passive NOx Adsorbers, Ind. Eng. Chem. Res. 2022, 61, 9, 3329–3341.

(74) Y. Ryou, J. Lee, H. Lee, C. H. Kim, D. H. Kim, Low temperature NO adsorption over hydrothermally aged Pd/CeO2 for cold start application, Catal. Today 2018, 307, 93-101.

(75) Ji, Y.; Xu, D.; Bai, S.; Graham, U.; Crocker, M.; Chen, B.; Shi, C.; Harris, D.; Scapens, D.; Darab, J.Pt- and Pd-Promoted CeO2–ZrO2 for Passive NOx Adsorber Applications, Ind. Eng. Chem. Res. 2017, 56, 1, 111–125.

(76) Z. Hong, Z. Wang, X. Li, Catalytic oxidation of nitric oxide (NO) over different catalysts: an overview, Catal. Sci. Technol., 2017,7, 3440-3452

(77) Zhang, L.; Spezzati, G.; Muravev, V.; Verheijen, M. A.; Zijlstra, B.; Filot, I. A. W.; Su, Y.-Q.; Chang, M.-W.; Hensen, E. J. M. Improved Pd/CeO2 Catalysts for Low-Temperature NO Reduction: Activation of CeO2 Lattice Oxygen by Fe Doping. ACS Catal. 2021, 11, 5614–5627

(78) Srinivasan, P.D.; Khivantsev, K.; Tengco, J.; Zhu, H.; Bravo-Suárez, J.J. Enhanced Ethanol Dehydration on gamma-Al2O3 Supported Cobalt Catalyst, Journal of Catalysis, 2019, 373, 276-296.

(79) Müller, P.; Hermans, I. Applications of Modulation Excitation Spectroscopy in Heterogeneous Catalysis. Ind. Eng. Chem. Res. 2017, 56, 1123– 1136.

(80) Ferri, D.; Kumar, M. S.; Wirz, R.; Eyssler, A.; Korsak, O.; Hug, P.; Weidenkaff, A.; Newton, First steps in combining modulation excitation spectroscopy with synchronous dispersive EXAFS/DRIFTS/mass spectrometry for in situ time resolved study of heterogeneous catalysts, Phys. Chem. Chem. Phys., 2010,12, 5634-5646.